Ferromagnetic resonance in coupled ultrathin films

2003 J. Phys.: Condens. Matter 15 S465

(http://iopscience.iop.org/0953-8984/15/5/303)

INSTITUTE OF PHYSICS PUBLISHING JOURNAL OF PHYSICS: CONDENSED MATTER

J. Phys.: Condens. Matter **15** (2003) S465–S478 PII: S0953-8984(03)54218-7

Ferromagnetic resonance in coupled ultrathin films

J Lindner[1] **and K Baberschke**

Institut für Experimentalphysik, Freie Universität Berlin, Arnimallee 14, D-14195 Berlin, Germany

E-mail: babgroup@physik.fu-berlin.de (J Lindner)

Received 2 October 2002
Published 27 January 2003
Online at stacks.iop.org/JPhysCM/15/S465

Abstract

Ferromagnetic resonance (FMR) is known to be one of the most informative techniques to measure basic physical quantities such as magnetic anisotropy energies, the g tensor in solids or the interlayer exchange coupling J_{inter}. We investigate prototype Cu/Ni/Cu/Ni/Cu(001) and Ni/Cu/Co/Cu(001) trilayers as well as Fe_n/V_m superlattices. We show for the case of trilayers how *in situ* ultrahigh vacuum FMR can be used to determine J_{inter} in absolute energy units in a straightforward way: we first prepare and measure the bottom magnetic layer together with the Cu spacer *in situ* and then evaporate the second magnetic film on top. Thus, it is possible to investigate the FMR signal before and after the two magnetic films become coupled. We discuss results, showing that the temperature dependence of J_{inter} follows a $T^{3/2}$ law over a wide temperature range. This indicates that thermally excited spin waves at the interface of the ferromagnetic layers dominate the temperature dependence of J_{inter}. The second part focuses on the measurement of the g value. From the g value, the ratio of orbital to spin magnetic moment can be obtained via the relation $\mu_L/\mu_S = (g-2)/2$. We show for Fe_n/V_m superlattices how μ_L/μ_S increases with decreasing Fe-layer thickness.

1. Introduction

Ferromagnetic resonance (FMR) has been a well established technique to determine anisotropies in ferromagnetic (FM) systems for more than 50 years [1]. The number of magnetic moments which are still detectable in an FMR experiment is in the order of 10^{10}–10^{14} depending on the linewidth of the signal. This corresponds to film thicknesses in the monolayer range. Due to its sensitivity, FMR has been successfully applied to ultrathin metallic films [2]. FMR can also be used to study the coupling between FM films separated by non-magnetic spacer layers, which can be metallic or non-metallic (for the non-metallic spacer layers, see [28]). This serves as a prototype to study multilayer exchange coupling, an

[1] Author to whom any correspondence should be addressed.

important focus when investigating electric transport properties in multilayer structures. To investigate this interaction, a technique is needed which allows us to measure the coupling in absolute units (e.g. in eV/particle). Unlike many other experimental methods, which only give a relative measure of the interaction, FMR was shown to yield absolute values [3]. To investigate the coupling from a fundamental point of view, it is also important to be able to construct the layered structure step-by-step in an ultrahigh vacuum (UHV) system.

In section 2 the principles of FMR in single (section 2.1) and coupled (section 2.2) ultrathin films is reviewed. Section 3 presents the experimental results for trilayers of $Ni_7Cu_xCo_2/Cu(001)$ and $Cu_4Ni_8Cu_xNi_9/Cu(001)$[2]. The combination of FMR in coupled systems and the use of a UHV environment is demonstrated. A detailed investigation of the coupling as a function of the spacer thickness is presented in section 3.1. In section 3.2 it is shown via temperature-dependent measurements over a wide temperature regime that the coupling exhibits a $T^{3/2}$ behaviour.

Another important quantity that can be addressed by FMR and is discussed in section 4 is the g value, which in solids becomes a tensor quantity. Unlike in paramagnetic samples, for a ferromagnet it is not only the external Zeeman field that affects the resonance condition. This makes it much more difficult to measure the components of the g tensor. Section 4 explains an experimental method which allows precise measurements of the g tensor components in FM solids. Section 4.1 illustrates this method by discussing results for the in-plane component $g_{\|}$ in the case of multilayered Fe/V samples.

2. FMR in ultrathin ferromagnets

2.1. FMR in single ultrathin films

Since the energy associated with microwave absorption lies in the μK range, FMR is the technique of choice to investigate the thermodynamic ground-state properties. The theory for FMR has been developed within a classical [1] and a quantum mechanical framework [4]. Due the large number of spins taking part in a resonance experiment, of the order of 10^{10}–10^{14}, both descriptions were shown to be equivalent [5]. It is therefore possible to describe the resonance phenomenon by applying a macroscopic equation of motion for the behaviour of the magnetization vector $\vec{M}$ formed by the magnetic moments in the sample. If, in addition, one considers single-domain magnetic films with thicknesses well below the ultrathin film limit, $\vec{M}$ can be assumed to be uniform throughout the sample. Within these assumptions, the equation of motion first derived by Landau and Lifshitz is

$$\frac{\mathrm{d}\vec{M}}{\mathrm{d}t} = -\gamma \vec{M} \times \left(\vec{H}_{eff} + \vec{H}_0 + \vec{h}_{rf}\right). \tag{1}$$

The expression on the right-hand side of equation (1) is the torque acting on the magnetization $\vec{M}$ which has been separated into parts arising due to the external ($\vec{H}_0$), the internal ($\vec{H}_{eff}$) and the high-frequency ($\vec{h}_{rf}$) fields respectively. $\gamma = g\mu_B/\hbar$ is the gyromagnetic ratio ($\gamma/2\pi = 2.8$ GHz kOe^{-1} for $g = 2$). Smit and Beljers have shown that the equation of motion may be expressed in terms of the total free energy density F instead of effective fields [6]. The first step is to calculate the equilibrium positions θ^0, φ^0 of the magnetization for a given external field value. For this the total free energy density F has to be a minimum, i.e. the equilibrium values can be obtained from the conditions $\partial F/\partial\theta = 0$ and $\partial F/\partial\varphi = 0$. Assuming small deviations from the equilibrium positions due to the presence of the driving radiofrequency (rf) field created by the microwaves with frequency ω, Smit and

[2] In the following the film thickness in monolayers (ML) is given as a subscript.

Beljers [6] derived a general formula which can be used to determine the resonance frequency as a function of the external field, once the contributions to F have been specified.

$$\left(\frac{\omega}{\gamma}\right)^2 - \frac{(F_{\theta\theta}F_{\varphi\varphi} - F_{\theta\varphi}^2)}{M^2 \sin^2\theta^0} = 0. \tag{2}$$

The derivatives of F with respect to θ and φ have to be taken at the equilibrium positions θ^0 and φ^0. For our systems of tetragonal symmetry, the free energy per unit volume is written in the form

$$\begin{aligned} F = &-MH_0\cos(\theta - \theta_H) + \left(2\pi M^2 - K_{2\perp}\right)\cos^2\theta - \frac{1}{2}K_{4\perp}\cos^4\theta \\ &- \tfrac{1}{8}K_{4\parallel}(3 + \cos 4\varphi)\sin^4\theta - K_{2\parallel}\cos^2(\varphi - \varphi_u)\sin^2\theta \end{aligned} \tag{3}$$

θ and θ_H are the polar angles of the magnetization and the external field measured from the film normal and φ and φ_H are the azimuthal angles measured with respect to the [100] in-plane direction. $K_{2\perp}$ gives the intrinsic out-of-plane anisotropy constant. A negative value indicates an easy direction in the film plane, whereas a positive value shows a preferential direction normal to the film plane. $K_{2\perp}$ is created by the tetragonal distortion of the film. For cubic systems such a contribution vanishes due to symmetry reasons. We will, however, show that all systems discussed in this paper are tetragonally distorted due to their pseudomorphic growth. $K_{2\parallel}$, the in-plane uniaxial term, is usually very small and may result from a slight mis-cut of the substrate which leads to a preferential direction in the film plane given by the angle φ_u. $K_{4\perp}$ and $K_{4\parallel}$ are the fourfold in- and out-of-plane anisotropy constants respectively. For Ni films they were shown to determine the continuous character of the reorientation transition of the easy axis of magnetization from the in- to the out-of-plane direction which was found in the Ni/Cu(001) system [2, 7]. The derivatives of equation (3) with respect to θ or φ are inserted into equation (2). For the case that the field is rotated in the plane given by the in-plane [110]-direction and the film normal, i.e. for the restriction $\varphi^0 = \varphi_H = 45°$, the following expression is derived

$$\begin{aligned} \left(\frac{\omega}{\gamma}\right)^2 = &\left[H_0\cos\Delta\theta + \left(M_{eff} + \frac{K_{4\perp}}{M} - \frac{K_{4\parallel}}{2M}\right)\cos 2\theta^0 + \left(\frac{K_{4\perp}}{M} + \frac{K_{4\parallel}}{2M}\right)\cos 4\theta^0\right] \\ &\times \left[H_0\cos\Delta\theta + \left(M_{eff} + \frac{K_{4\perp}}{M} - \frac{K_{4\parallel}}{2M}\right)\cos^2\theta^0 \right. \\ &\left. + \left(\frac{2K_{4\perp}}{M} + \frac{K_{4\parallel}}{M}\right)\cos^4\theta^0 - \frac{2K_{4\parallel}}{M}\right] \end{aligned} \tag{4}$$

where $\Delta\theta = \theta^0 - \theta_H$ and $M_{eff} = 2K_{2\perp}/M - 4\pi M$ are used. Equation (4) can be used to analyse out-of-plane angular dependence and shows that, except for $K_{2\parallel}$, all anisotropy constants influence the functional behaviour for the out-of-plane case.

2.2. FMR in coupled ultrathin films

This section explains how the analysis for a single film is extended to a trilayer consisting of two magnetic layers which are separated by a paramagnetic spacer layer. The method of Smit and Beljers can still be used in the case of coupled films to show its general character. The coupling energy U_{ex} of the two films 1 and 2 is added to the expression for F (equation (3)) via the term

$$U_{ex} = -J_{inter}\frac{\vec{M}_1 \cdot \vec{M}_2}{M_1 M_2} \tag{5}$$

where J_{inter} is the interlayer coupling parameter. In equation (5), J_{inter} appears formally in the same way as the Heisenberg-exchange integral describing the coupling between two individual spins in *one* magnetic film. However, J_{inter} has to be distinguished from the temperature-independent exchange constant within the Heisenberg interaction. It is, in fact, an averaged macroscopic quantity which measures the energy difference between parallel and antiparallel alignment of the two magnetizations $\vec{M}_1$ and $\vec{M}_2$. After introducing the coupling term via equation (5) one gets from the Smit and Beljers method

$$\left(\frac{\omega}{\gamma}\right)^4 - b\left(\frac{\omega}{\gamma}\right)^2 + c = 0. \tag{6}$$

Thus, for the coupled system one has a similar expression as for the single film (equation (2)). The constants b and c are now given by

$$b = \frac{F_{\theta_1\theta_1}F_{\varphi_1\varphi_1} - F^2_{\theta_1\varphi_1}}{d_1^2M_1^2\gamma_2^2\sin^2\theta_1^0} + \frac{F_{\theta_2\theta_2}F_{\varphi_2\varphi_2} - F^2_{\theta_2\varphi_2}}{d_2^2M_2^2\gamma_1^2\sin^2\theta_2^0} + 2\frac{F_{\theta_1\theta_2}F_{\varphi_1\varphi_2} - F_{\theta_1\varphi_2}F_{\theta_2\varphi_1}}{d_1d_2M_1M_2\gamma_1\gamma_2\sin\theta_1^0\sin\theta_2^0} \tag{7}$$

$$\begin{aligned} c = \frac{1}{d_1^2d_2^2M_1^2M_2^2\sin^2\theta_1^0\sin^2\theta_2^0}\big[&F^2_{\theta_1\theta_2}F^2_{\varphi_1\varphi_2} + F^2_{\theta_1\varphi_1}F^2_{\theta_2\varphi_2} + F^2_{\theta_1\varphi_2}F^2_{\theta_2\varphi_1} \\ &- F^2_{\theta_1\theta_2}F_{\varphi_1\varphi_1}F_{\varphi_2\varphi_2} - F^2_{\varphi_1\varphi_2}F_{\theta_1\theta_1}F_{\theta_2\theta_2} - F^2_{\theta_2\varphi_2}F_{\theta_1\theta_1}F_{\varphi_1\varphi_1} - F^2_{\theta_1\varphi_2}F_{\theta_2\theta_2}F_{\varphi_1\varphi_1} \\ &- F^2_{\theta_2\varphi_1}F_{\theta_1\theta_1}F_{\varphi_2\varphi_2} + F_{\theta_1\theta_1}F_{\varphi_1\varphi_1}F_{\theta_2\theta_2}F_{\varphi_2\varphi_2} + 2F_{\theta_1\theta_1}F_{\varphi_1\varphi_2}F_{\theta_2\varphi_2}F_{\theta_2\varphi_2} \\ &+ 2F_{\theta_1\varphi_1}F_{\theta_1\varphi_2}F_{\varphi_1\varphi_2}F_{\theta_2\theta_2} + 2F_{\theta_1\theta_2}F_{\theta_1\varphi_2}F_{\varphi_1\varphi_1}F_{\theta_2\varphi_2} + 2F_{\theta_1\theta_2}F_{\theta_1\varphi_1}F_{\theta_2\varphi_1}F_{\varphi_2\varphi_2} \\ &- 2F_{\theta_1\varphi_1}F_{\theta_2\varphi_2}\left(F_{\theta_1\theta_2}F_{\varphi_1\varphi_2} + F_{\theta_1\varphi_2}F_{\theta_2\varphi_1}\right) - 2F_{\theta_1\theta_2}F_{\varphi_1\varphi_2}F_{\theta_1\varphi_2}F_{\theta_2\varphi_1}\big]. \end{aligned} \tag{8}$$

Despite its complex form, equation (6) allows us to analyse angular dependences for coupled systems. The difference between the signals of two single films which are uncoupled and a coupled system is shown in figure 1 for the special case that $\vec{H}_0$ is applied in the film plane. The solid lines indicate the signals of two slightly different magnetic films which do not interact. This would be the situation for two films separated by an infinitely large spacer layer, where both films have their individual resonance fields that can be described by equation (4). When the spacer thickness is reduced, the two films become coupled. As shown by the dashed lines, the coupled system presents two eigenmodes formed by the uniform modes of the individual films. For the acoustical mode both magnetizations precess in-phase, whereas for the weaker optical mode they rotate out-of-phase. The relative positions of optical and acoustical mode can be used to identify the sign of J_{inter}, since figure 1 shows that for FM (antiferromagnetic (AFM)) coupling the acoustical mode is located at higher (lower) fields than the optical mode. Furthermore, the exact mode positions reflect the absolute value of J_{inter} when they are analysed in the context of equation (6). The appearance of two eigenmodes is similar to the case of two coupled pendula. This analogy also explains that, unless the two magnetic films are identical (see below), *both* eigenmodes have resonance fields which are different from the ones for the uncoupled films. Moreover, it is important to note that the coupled modes do not belong to one film only. They merely arise from both magnetic layers. Figure 1 further shows that for larger values of J_{inter} the intensity ratio between optical and acoustical mode decreases (dotted curves)—independent of its sign. This means that with increasing J_{inter} more oscillator strength is coupled to the acoustical mode, while the oscillator strength for the optical mode becomes weaker.

Figure 1 shows an alternative way of deducing J_{inter}. Compared to the uncoupled H_{res} values, both modes move towards higher (lower) field values within the coupled system for AFM (FM) coupling. This shift can also be taken as a measure of J_{inter}, provided that at least one H_{res} value for $J_{inter} = 0$ is known. The advantage of this method is that it is no longer

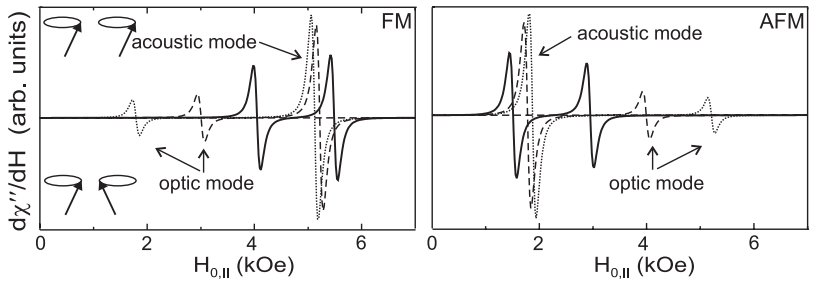

Figure 1. Simulation of the FMR signals according to equation (6) for two uncoupled ultrathin films (solid curves) and for the same films after FM and AFM coupling has been introduced (dashed curves). The dotted curves show the spectra after the coupling has been doubled.

important to observe both modes in the coupled system. This is particularly useful for strong coupling, where the optical mode becomes weaker and is therefore not always observable.

Finally, the case of two *identical* magnetic layers is discussed; this case is easily explained via the analogy of the coupled pendula. If both pendula are identical, no force is exerted on the pendula by the coupling spring during the in-phase oscillation, so that the oscillation frequency is unchanged from that of the single pendulum. Thus, in the trilayer the acoustical mode would stay unaltered and present the same H_{res} as the single individual layers, whereas the H_{res} of the optical mode would still be changed.

3. Interlayer coupling: absolute determination of J_{inter} using *in situ* FMR

In the following we show how *in situ* FMR can be used to investigate trilayer systems by applying the second method explained in the previous section. This approach allows us to measure and thus compare the *same* film before and after the deposition of each layer. We explain this procedure via a specific example of a $Cu_4Ni_8Cu_5Ni_9$/Cu(001) trilayer. The first step is to evaporate the bottom 9 ML thick Ni film already capped with 5 ML of Cu. Details concerning the film preparation and the well known epitaxial growth of the Ni/Cu(001) system may be found elsewhere [8–10]. The dashed curve in figure 2(a) shows the signal of the Cu_5Ni_9 film measured along the in-plane direction, i.e. at $\theta_H = 90°$ (for better clarity only part of the full resonance signal is displayed). Figure 2(b) shows the complete angular dependence of H_{res} measured for this film at $T = 294$ K before (dashed curve) and (solid curve) after capping with 5 ML of Cu. One sees that the minimum for H_{res} occurs at $\theta_H = 90°$ for the bare Ni film, whereas after depositing Cu on the same film the minimum is shifted to $\theta_H = 0°$. This indicates that the easy direction of magnetization has switched from being in the film plane towards the film normal. This effect is explained by a shift of the reorientation transition for the Ni/Cu(001) system upon changing the topmost surface due to the presence of an overlayer. Details of this effect are discussed in [11]. By fitting the angular dependences in figure 2(b) to equation (4), all anisotropy constants can be obtained. The switching of the easy axis of magnetization can be seen in the change of sign observed for M_{eff}. The fourth-order constants were found to have negative signs. This indicates an in-plane easy axis along the [110] direction and is well known for the Ni/Cu(001) system in this thickness range. For our Ni thicknesses the values of the fourth-order terms are, however, by a factor of 10 smaller than the perpendicular term, so that they are neglected (for the fundamental importance of higher-order constants for the Ni/Cu(001) system, see [2, 7, 12]). Now, knowing the anisotropies of the Cu capped Ni film, we will, in the next step, deposit a second Ni film on top. The resulting FMR spectrum for the trilayer measured at room temperature is shown as a thick solid curve in figure 2(a). In the trilayer one observes

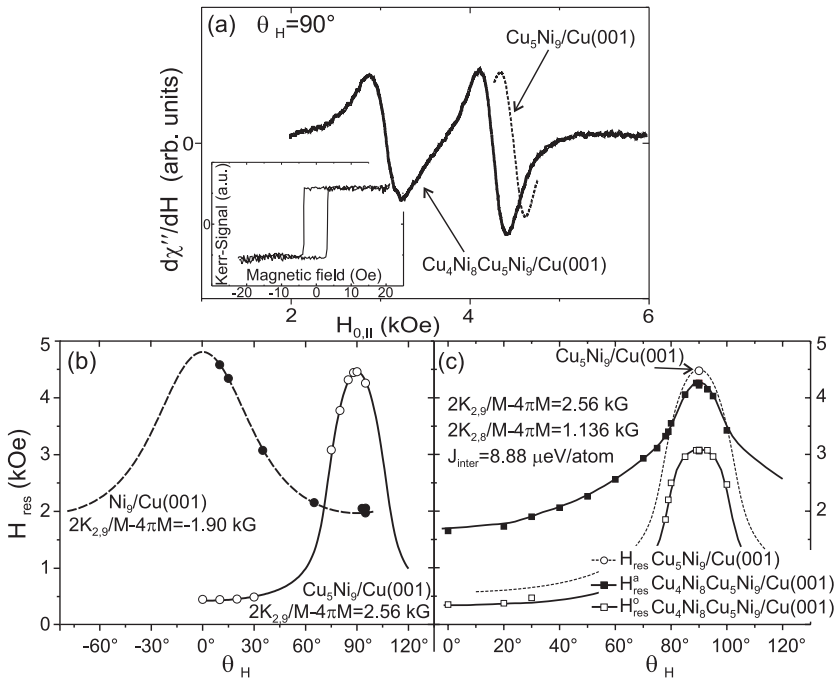

Figure 2. (a) FMR spectra for Cu_5Ni_9/Cu(001) before (dashed curve) and after depositing the topmost Cu_4Ni_8 layers. (b) Angular dependence for Cu_5Ni_9/Cu(001) with (solid curve) and without (dashed curve) a Cu cap layer. (c) Angular dependence measured for optical (open squares) and acoustical (solid squares) modes in the $Cu_4Ni_8Cu_5Ni_9$/Cu(001) trilayer. The dashed curve is the same dependence shown in (b) for the Cu-capped bottom film only.

two resonances. The larger acoustical mode with resonance field H^a_{res} is located at higher fields with respect to the optical mode (H^o_{res}) and thus the system is coupled ferromagnetically. This is confirmed by the polar MOKE results from the same trilayer shown in the inset. One observes a rectangular loop indicating that the two magnetizations flip together due to their FM coupling. Besides the sign of the coupling, however, the Kerr effect does not allow us to deduce the value of J_{inter}. In addition, H^a_{res} is shifted to lower fields with respect to that of the bottom film (dashed curve). This situation has to be compared with the FM case of figure 1, thus also indicating the FM coupling. To unambiguously extract J_{inter} from the field shift or from the two mode positions, one needs to know the anisotropy values for the *two* Ni films, since they influence the shift and thus the positions. The values for the first film have already been determined. Figure 2(c) shows how the K values of the topmost Cu_4Ni_8 film are determined from the full angular dependence in the *coupled* system. The experimental values of the optical (open squares) and acoustical mode (solid squares) are shown together with a fit according to equation (6). One obtains a value of 1.136 kG for M_{eff}, which is smaller than that found for the bottom film due to the lower thickness of the topmost layer. The positive value also indicates that the topmost film has an easy axis along the film normal. It is interesting to note that the angular dependence in coupled trilayers is in principle different from that known from single films. If the two films were uncoupled their different anisotropies would imply that one film has the larger H_{res} along the hard direction, but also the smaller H_{res} along the easy axis. This would then lead to a crossing of the two angular dependences at a particular angle. The dependences of optical and acoustical modes, however, do not cross, i.e. for *all* θ_H values the optical

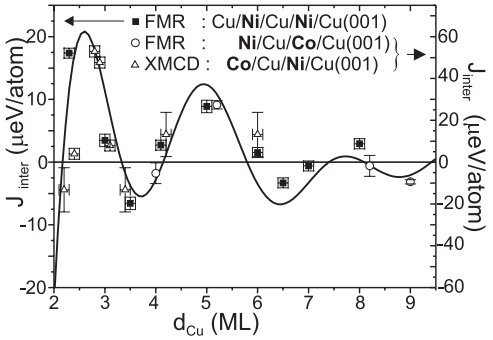

Figure 3. J_{inter} as a function of the spacer thickness d_{Cu}.

mode is located at lower H_{res} values reflecting the FM coupling of the films. Taking the angular dependences of the bottom film only and the one measured in the coupled system, *all* unknown values influencing the H_{res} of optical and acoustical modes can be eliminated. Then, the only parameter left which determines the shift is J_{inter} itself. This straightforward way of determining the coupling in absolute units demonstrates the tremendous advantage of measuring *in situ* and thus yields a very precise measure of J_{inter}. In the following, we discuss parameters that influence J_{inter} and can be used to tune the coupling between two magnetic layers.

3.1. J_{inter} as a function of the spacer thickness

In figure 3, J_{inter} is plotted in absolute units as a function of the spacer thickness for Cu/Ni/Cu/Ni/Cu(001) (squares) and Ni/Cu/Co/Cu(001) (open circles) trilayers. Positive values of J_{inter} indicate FM, negative values AFM coupling. Note that the right axis corresponds to the Ni/Cu/Co/Cu(001) system for which much larger coupling is found. One clearly sees an oscillatory behaviour of J_{inter} as a function of the spacer thickness which is attenuated for larger d_{Cu}. According to the theory of Bruno [13] one can write the coupling as

$$\frac{J_{inter}}{J_{inter,0}} \sim \frac{1}{d_{\mathrm{Cu}}^2} \sum_j \sin(k_j^s \cdot d_{\mathrm{Cu}} + \phi_j). \tag{9}$$

Here $J_{inter,0}$ is the value of J_{inter} at $T = 0$ K, the k_j^s give the oscillation periods, ϕ_j are the phases and d_{Cu} is the spacer thickness. Equation (9) shows that the oscillation periods of the coupling depend only on the characteristics of the Fermi surface of the spacer material and are given by extremal spanning vectors of the Fermi surface k_j^s [13, 14]. For Cu(001), periods of 2.56 and 5.88 ML are predicted. The solid line in figure 3 is the predicted curve using these two periods and phases for Cu(001). Note that the only adjustable parameters which were scaled to match the absolutely measured data points are the two amplitudes giving the strength of the coupling. Thus, FMR provides an important tool to correlate experimental data with theoretical work which usually does not provide the amplitudes of the oscillations. The open triangles are results for Co/Cu/Ni/Cu(001) trilayers taken from [15]. The results were obtained using x-ray magnetic circular dichroism (XMCD). Due to the excitation of *localized* 2p electrons into the exchange split 3d bands, XMCD is element-specific and allows us to measure the magnetization curves of the two FM layers separately [15]. Upon depositing the topmost Co layer, the coupling leads to a shift of T_C^{Ni} to higher values from which J_{inter} can be deduced. Since this analysis provides only relative values, a simple mean-field approach was used in [15] to translate the T_C shift into absolute values of J_{inter}. This procedure results, however, in values which are about two orders of magnitude too large so that it was necessary

to scale the XMCD data in figure 3 on the y axis to match the correct values obtained by FMR. Figure 3 shows that after this scaling the results from both techniques are in excellent agreement concerning the oscillatory behaviour.

3.2. Temperature dependence of J_{inter}

The difference between J_{inter} and a Heisenberg exchange can be seen from the fact that it is strongly temperature dependent. Since J_{inter} measures the coupling strength, it is all important to understand the mechanisms which leads to its temperature dependence. In a previous experiment [16] the temperature dependence of J_{inter} of Co/Ru/Co trilayers was determined only within a very small range in reduced temperature $t = T/T_C$. Here we will show that it is important to measure over a large temperature range, if possible from $T = 0$ K up to the Curie temperature. Above T_C no ferromagnetism exists and, consequently, no coupled spin wave excitations are possible.

There exist, basically, the following two different mechanisms to explain the temperature dependence of the interlayer coupling.

(i) Thermally excited spin waves in the magnetic layers lead to a reduction of the effective interlayer exchange [17]. In this model the characteristic temperature defining the temperature dependence is given by T_C, and J_{inter} as a function of T has the form

$$\frac{J_{inter}}{J_{inter,0}} = 1 - a\left(\frac{T}{T_C}\right)^{3/2} \tag{10}$$

where a is of order unity [17].

(ii) Thermal excitations of electron–hole pairs across the Fermi level in the spacer material [13, 18] are described by the rounding of the Fermi–Dirac distribution function at elevated temperatures which leads to a decrease of the effective coupling between the magnetic layers given by

$$\frac{J_{inter}}{J_{inter,0}} = \frac{T/T_0}{\sinh\left(\frac{T}{T_0}\right)} \tag{11}$$

where $T_0 = (\hbar v_F)/(2\pi k_B d)$ is the value which determines the functional behaviour. v_F, the only temperature-dependent quantity within T_0, is the Fermi velocity of the carriers in the spacer with thickness d. In this model the coupling does not vanish necessarily at the Curie temperature T_C. Large Fermi velocities v_F, i.e. large T_0 values, decrease the effective temperature dependence. Since, in particular for noble metal spacers, v_F is quite large (about 10^8 cm s^{-1}) only a small temperature dependence in the range 1–1000 K can be expected. Another quantity which does not enter explicitly into model (i) is d. According to model (ii) larger spacer thicknesses lead to a more pronounced temperature dependence. Both models will now be compared with our experimental results for $Ni_7Cu_xCo_2$/Cu(001) trilayers with $x = 5, 9$ ML. From figure 3 it can be seen that the trilayer with $x = 5$ ML is coupled ferromagnetically, whereas the trilayer with $x = 9$ ML is coupled antiferromagnetically. The FMR spectra of the trilayer with $x = 9$ ML for the lowest temperature of $T = 55$ K and for room temperature measured along the in-plane [110] direction are presented in figures 4(c) and (d). The dotted spectra result from the bottom Co film already being capped with the Cu spacer. Since H_{res} is located at low field values, the magnetization lies in the film plane. The shift of H_{res} to higher fields at room temperature is due to the reduction of the anisotropies. In the spectrum for the trilayer at $T = 55$ K, the shift of the resonance to larger fields indicates the AFM coupling. However, due to the strong coupling only the acoustical mode is observable. The possibility to still determine J_{inter} shows the advantage of the *in situ* approach. At room

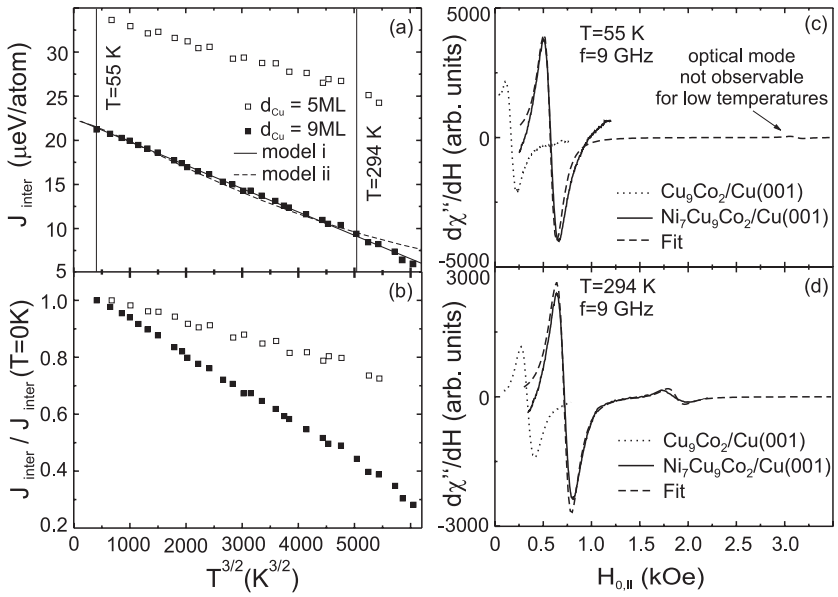

Figure 4. (a) J_{inter} as a function of $T^{3/2}$ for $Ni_7Cu_xCo_2$/Cu(001) trilayers with $x = 5, 9$. (b) Temperature dependence shown in (a) normalized to the value of J_{inter} at $T = 0$ K. (c) and (d) Spectra at $T = 55$ and 294 K respectively.

temperature both modes appear, indicating that J_{inter} is reduced. The complete temperature dependence of J_{inter} is displayed in the left panel of figure 4 where J_{inter} is plotted as a function of $T^{3/2}$ for the two cases. In (a) absolute units and in (b) J_{inter} normalized to the extrapolated $T = 0$ K value are shown. For both trilayers one can clearly see a linear dependence over a wide temperature range. In addition, it was shown in [20] that a fit according to model (ii) shows reasonable agreement only if unrealistic small values for v_F are used. The best fit shown by the dashed line in figure 4 is obtained for $v_F = 1.4 \times 10^7$ cm s^{-1} which is by a factor of 10 smaller than the free electron value for Cu bulk ($v_F = 1.57 \times 10^8$ cm s^{-1}) and still by a factor of five smaller than realistic values determined experimentally by de Haas–van Alphen measurements yielding $v_F = 6.7 \times 10^7$ cm s^{-1} [19]. Thus, for both systems the main source of the temperature dependence in J_{inter} results from spin wave excitations. Model (i) was even shown to hold for a multilayered Fe/V structure as discussed in [20]. Besides the fact that both systems in figure 4 show a linear behaviour in the $T^{3/2}$ plot, a difference between the two trilayers is observed. One finds that the temperature dependence, despite being linear, is stronger for the trilayer with the larger spacer thickness, as can be seen in (b). Model (i) does not give an explanation for this behaviour, whereas model (ii) explicitly predicts this trend. This experimental finding thus shows that more theoretical work is needed to understand such a dependence on the spacer thickness within model (i). In particular, the origin of the constant a, which is not discussed in [17], needs to be specified.

4. Orbital magnetism: determination of the g value in FM ultrathin films

In the following, a method is explained that allows us to determine the g value in FM samples. The g value can be related to the ratio of orbital to spin moment via [21]

$$\frac{\mu_L}{\mu_S} = \frac{g-2}{2}. \tag{12}$$

Thus, the departure from $g = 2$ is a measure of the orbital contribution. Moreover, once the total moment $\mu = \mu_L + \mu_S$ is measured (e.g. via SQUID [22]), one can determine μ_L. The quenching of the orbital momentum in cubic symmetry leads to g values very close to $g = 2$. Lower crystallographic symmetry and spin–orbit coupling reinstalls orbital magnetism, leading to $g \geqslant 2$ for more than half-filled 3d elements. It is well known that for the bulk ferromagnets Fe, Co and Ni the g values are $g_{\mathrm{Fe}} = 2.09$, $g_{\mathrm{Co}} = 2.18$ and $g_{Ni} = 2.21$ (see also [29]). In addition, the lower symmetry of the crystal field results in the fact that in a solid the g value in general becomes a tensor quantity. g becomes a symmetrical tensor of second rank with g_x, g_y and g_z being the principal values. For tetragonal, trigonal and any kind of axial symmetry, $g_x = g_y = g_\parallel$ and $g_z = g_\perp$. For cubic symmetry $g_\perp = g_\parallel$, so that for bulk Fe and Ni the g tensor is isotropic. In thin films, the deviation of the crystallographic structure from cubic symmetry is caused by the pseudomorphic growth leading to a lower symmetry.

At first glance, the determination of the g value in ultrathin FM films seems to be straightforward. By fitting angular-dependent measurements to equation (4) the gyromagnetic ratio γ and thus g can be obtained. The disadvantage of this method, however, is that the anisotropy constants also have to be fitted at the same time. A way to solve this problem is to combine both angular dependences at different microwave frequencies. Then, all anisotropy constants can be determined independently. However, this approach is also problematic, since the uncertainty of the anisotropies enters into the determination of g. A way to circumvent this problem was discussed in [23].

The resonance condition of a tetragonal system given by equation (4) for the in-plane [110] direction takes the form

$$\left(\frac{\omega}{\gamma_\parallel}\right)^2 = H_{0\parallel}^2 + H_{0\parallel}\left(M_{eff} - \frac{K_{4\parallel}}{M}\right) - 2\frac{K_{4\parallel}}{M}\left(M_{eff} + \frac{K_{4\parallel}}{M}\right). \tag{13}$$

For the in-plane [100] direction the only difference is that the $K_{4\parallel}/M$ terms on the right-hand side of the equation have to be replaced by $+4K_{4\parallel}/M$ (first brackets), $+2K_{4\parallel}/M$ (before second brackets) and $+2K_{4\parallel}/M$ (last brackets). For the perpendicular configuration one obtains from equation (4)

$$\frac{\omega}{\gamma_\perp} = H_{0\perp} + \left(M_{eff} + 2\frac{K_{4\perp}}{M}\right). \tag{14}$$

The two dependences are illustrated schematically in figure 5(a), where f^2 as a function of $H_{0\parallel}$ and f as function of $H_{0\perp}$ are plotted. A parabolic behaviour is expected for the in-plane components $g_{\parallel,[110]}$ and $g_{\parallel,[100]}$ while the perpendicular component $g_\perp$ follows a linear dependence. By using several frequencies, the experimental points can be fitted to equations (13) and (14). As a result, the only parameter that influences the slope for the perpendicular orientation and the prefactor of the term quadratic in $H_{0\parallel}$ for the in-plane directions is the gyromagnetic ratio, i.e. g. Consequently, g can be determined independently of the anisotropy values.

4.1. $g_\parallel$ in Fe/V superlattices

To illustrate the multifrequency approach, we will discuss results for prototype 3d-based $\mathrm{Fe}_n/\mathrm{V}_m$ superlattices (SLs) with $n = 2, 4$ and $m = 2, 4, 5$. $\mathrm{Fe}_n/\mathrm{V}_m$ SL can be grown with very high structural [24] as well as magnetic homogeneity [25] in bcc(001) orientation on MgO substrates. The growth proceeds in a 2D Frank–Van der Merve fashion resulting in sharp interfaces with a typical roughness of only 2 Å. A RHEED investigation revealed an in-plane cubic structure. The Fe/V system presents an average out-of-plane lattice constant of about 2.9 Å which increases with increasing content of V. This value lies in-between the one

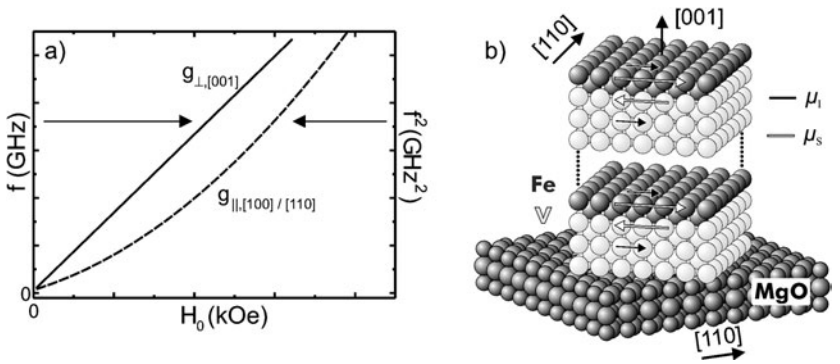

Figure 5. (a) Theoretical behaviour $f^2(H_{0\|})$ along the in-plane directions and $f(H_{0\perp})$ for the perpendicular orientation. (b) Schematic drawing of a Fe/V SL.

for bulk Fe (2.87 Å) and V (3.03 Å) and thus the magnetic Fe layers are slightly expanded along the out-of-plane direction leading to a tetragonal symmetry. Since SLs with thin Fe layers are expected to differ most from bulk properties, we have investigated a $(Fe_4/V_4)_{45}$ SL, a $(Fe_4/V_2)_{60}$ SL and a $(Fe_2/V_5)_{50}$ SL. Therefore, we can discuss the influence of decreasing the Fe thickness as well as the effect of decreasing the V thickness. Before discussing the g-value measurements, we briefly discuss at this point the important features of the three samples. A detailed presentation of the FMR measurements concerning the anisotropy values will be given elsewhere [26].

(i) Coupling between the Fe layers. The coupling between the Fe layers was found to be FM for all the three samples as consistently shown by XMCD [27], FMR and vibrating sample magnetometry (VSM). As shown for the special case of the trilayer in section 2.2, the coupling between the magnetic layers does not alter the resonance field of the acoustical mode compared to the resonance fields of the single magnetic layers for the case where the individual layers are identical. In addition, the intensity of the acoustical mode is large, whereas for identical layers the optical mode intensity is zero. Translated to the Fe/V SL, one expects a strong acoustical mode which reflects the collective coherent precession of the layers. Since each layer means one degree of freedom, $N-1$ optical modes are possible, N being the repetition of the SL period. However, the SL periods are nominally the same, so that ideally no intensity should be coupled with the optical modes. Indeed, only one mode was found at low frequencies. Only at frequencies larger than 17 GHz could small optical modes be observed. This finding implies that the SLs consist of almost perfectly symmetric SL periods and that one can analyse the acoustical mode by equation (4), i.e. via the equation derived for a single magnetic layer.

(ii) Coupling between Fe and V. It was shown via XMCD that the V layers also carry a magnetic moment in the Fe/V system [27]. Details of the XMCD measurements and the data analysis are presented in [27]. The separate determination of only the Fe magnetic moments can be done via XMCD with the help of the so-called sum rules. This procedure is well established for Fe. For V, however, the application of the sum rules is questionable because of the small spin–orbit splitting of the initial 2p core levels which leads to an considerable overlapping of the signal at the L_2 and L_3 edge. Thus, the V moments were deduced by taking the total moment obtained from VSM measurement and subtracting the Fe moments. The results are summarized in table 1. It can be seen that the total Fe (μ_{Fe}) and V (μ_V) moments are aligned antiparallel for all samples, consistent with theory (this

Table 1. Total magnetic moments and the ones for Fe and V only for the different Fe/V samples from [27] given in μ_B/atom. The g value of the $(Fe_2/V_5)_{50}$ SL results are from [23].

Sample	μ_{tot}	μ_{Fe}	μ_V	$g_{\parallel,[110]}$	$g_{\parallel,[100]}$
40 nm Fe		2.22			
$(Fe_4/V_2)_{60}$	1.59	2.12	−1.06	2.115(7)	2.109(12)
$(Fe_4/V_4)_{45}$	1.28	1.70	−0.42	2.134(9)	2.136(16)
$(Fe_2/V_5)_{50}$	0.67	1.34	−0.27	2.264(15)	

is indicated by the negative sign of μ_V). Moreover, it was shown in [27] that, although the spin moments of the Fe and V layers are oriented antiparallel, the orbital moments are all aligned parallel. The directions of orbital and spin magnetic moments within the different layers are indicated by arrows in figure 5(b) where a hard sphere model of a Fe/V SL is schematically shown.

The induced magnetism in V has consequences in analysing the FMR data, since the V layers also participate in the FMR in the Fe/V system. As a result, the two antiferromagnetically coupled sublattice magnetizations $M_{Fe} = n_{Fe}\mu_{Fe}$ and $M_V = n_V\mu_V$ precess together about the effective field direction, i.e. the system behaves as a ferrimagnet. Since the V and Fe layers are in direct contact, the coupling is much stronger than the weak interlayer coupling discussed in section 3. Thus, only the in-phase precession can be excited in the microwave regime, whereas the out-of-phase mode usually is observed in the far-infrared region. It is important to note that the in-phase mode which is of relevance here can still be described by equation (1) when one replaces M by the net magnetization of the two sublattices and g by an effective g_{eff} value. In this so-called 'FM limit', the ferrimagnetic system can thus be described as a ferromagnet with g_{eff} given by

$$\frac{n_{Fe}\mu_{Fe} + n_V\mu_V}{g_{eff}} = \frac{n_{Fe}\mu_{Fe}}{g_{Fe}} + \frac{n_V\mu_V}{g_V}. \tag{15}$$

The FMR results of g_{eff} for the different Fe/V SLs will now be discussed. Figure 6(a) shows FMR spectra for the $(Fe_4/V_2)_{60}$ and $(Fe_4/V_4)_{45}$ SLs for three different frequencies. One sees that with increasing frequency the resonance fields also become larger. The same trend is found for the $(Fe_2/V_5)_{50}$ SL. The results for this SL are taken from a previous measurement presented in [23] and are shown for two frequencies in figure 6(b). Upon plotting the frequencies squared as a function of the resonance fields for all frequencies as discussed in figure 5(a), one ends up with the result shown in figure 6(c). The result for the $(Fe_2/V_5)_{50}$ SL is plotted separately in the inset. One should note that in [23] only three different frequencies were available, whereas for the two other SLs seven different frequencies were used. One can see that this large range in frequency makes it possible to distinguish between the two samples. In particular at high-frequency values the resonance fields become significantly different from each other. As a consequence, the error in determining the g factor becomes much smaller. The fit according to equation (13), which shows a very good agreement with the data, yields the values for $g_{\parallel,[110]}$. The results are summarized in table 1. By decreasing the Fe thickness and increasing the V thickness, $g_{\parallel,[110]}$ also becomes progressively larger, indicating a larger ratio of orbital to spin magnetic moment. In [27] it was shown that this is most likely due to hybridization which influences both spin and orbital moment, when decreasing the Fe thickness. The orbital contribution, however, is not strongly affected because of its unquenching at small Fe thicknesses which leads to a partial compensation of the hybridization effect. Within the experimental error, no difference was found for the other in-plane component $g_{\parallel,[100]}$, also given in table 1. As stated above, this is expected for

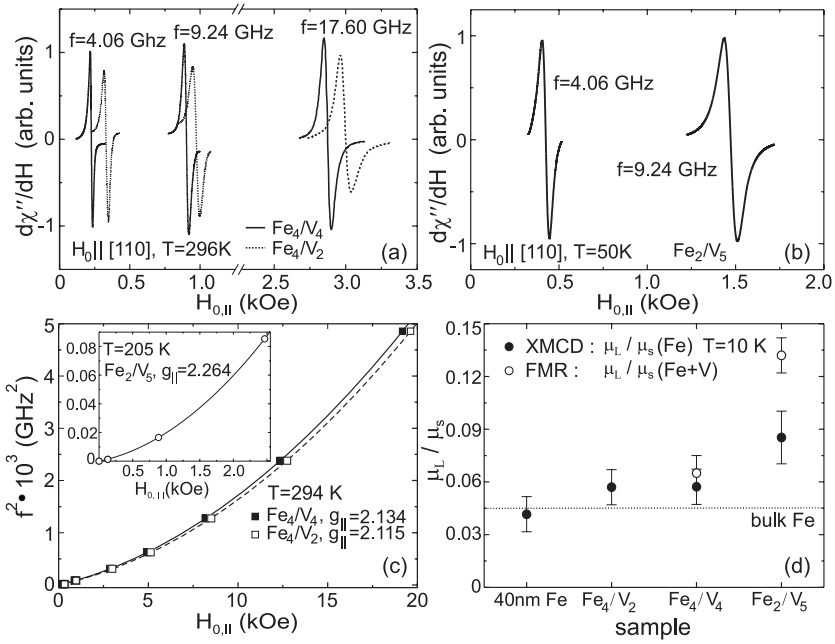

Figure 6. (a) and (b) FMR spectra for the Fe/V SLs at various frequencies. (c) Frequency squared as a function of $H_{0\|}$ applied parallel to the [110] direction. (d) Ratio of orbital to spin magnetic moment measured via FMR and XMCD.

tetragonal symmetry. Figure 6(d) shows μ_L/μ_S for the different samples obtained from the $g_{\|,[110]}$ values by using equation (12). Together with the results from FMR, μ_L/μ_S for Fe only as obtained from XMCD measurements on the same samples are shown. XMCD reveals that all samples present an enhanced orbital magnetism. While the $(Fe_4/V_2)_{60}$ shows a nearly bulk-like behaviour (dotted curve), the $(Fe_2/V_5)_{50}$ presents an orbital contribution of about 9% compared to 4.5% in bulk Fe. In addition, the FMR values lie systematically above the ones found via XMCD. This is the consequence of the fact that the orbital moments of the Fe and V layers add up, whereas the spin moments partially cancel out (see figure 5(b)). This shows that for systems with polarizable elements one has to take the response of the induced moments into account, i.e. the g values measured via FMR are given by equation (15).

Acknowledgments

This work was supported by the DFG, Sfb 290 and BMBF(05KS1 KEB4). E Kosubek, A Anisimov and C Rüdt are acknowledged for assistance during the FMR measurements. The high-frequency FMR results were obtained by D Spoddig and R Meckenstock. A Scherz and H Wende are acknowledged for performing the XMCD measurements. P Poulopoulos, D L Mills, B Heinrich and P Bruno are acknowledged for fruitful discussions and K Lenz for assistance in preparing the manuscript.

References

[1] Kittel C 1947 *Phys. Rev.* **73** 155
[2] Farle M 1998 *Rep. Prog. Phys.* **61** 755 and references therein
[3] Heinrich B and Cochran J F 1993 *Adv. Phys.* **42** 523

[4] Polder D 1948 *Phys. Rev.* **73** 1116
[5] Luttinger J M and Kittel C 1948 *Helv. Phys. Acta* **21** 480
[6] Smit J and Beljers H G 1955 *Phillips Res. Rep.* **10** 113
[7] Schulz B and Baberschke K 1994 *Phys. Rev.* B **50** 13467
[8] Heinz K, Müller S and Hammer L 1999 *J. Phys.: Condens. Matter* **11** 9437
[9] Lindner J, Kollonitsch Z, Kosubek E, Farle M and Baberschke K 2001 *Phys. Rev.* B **63** 094413
[10] Poulopoulos P, Lindner J, Farle M and Baberschke K 1999 *Surf. Sci.* **437** 277
[11] van Dijken S, Vollmer R, Poelsema B and Kirschner J 2000 *J. Magn. Magn. Mater.* **210** 316
[12] Poulopoulos P and Baberschke K 1999 *J. Phys.: Condens. Matter* **11** 9495
[13] Bruno P 1995 *Phys. Rev.* B **52** 411
[14] Stiles M D 1993 *Phys. Rev.* B **48** 7238
[15] Ney A, Wilhelm F, Farle M, Poulopoulos P, Srivastava P and Baberschke K 1999 *Phys. Rev.* B **59** R3938
[16] Zhang Z, Zhou L, Wigen P E and Ounadjela K 1994 *Phys. Rev. Lett.* **73** 336
[17] Almeida N S, Mills D L and Teitelman M 1995 *Phys. Rev. Lett.* **75** 733
[18] Drchal V, Kudrnovský J, Bruno P, Turek I, Dederichs P H and Weinberger P 1999 *Phys. Rev.* B **60** 9588
[19] Persat N and Dinia A 1997 *Phys. Rev.* B **56** 2676
[20] Lindner J, Rüdt C, Kosubek E, Poulopoulos P, Baberschke K, Blomquist P, Wäppling R and Mills D L 2002 *Phys. Rev. Lett.* **88** 167206
[21] Kittel C 1949 *Phys. Rev.* **76** 743
Kittel C 1951 *J. Phys. Radium* **12** 291
[22] Ney A, Poulopoulos P and Baberschke K 2001 *Europhys. Lett.* **54** 820
[23] Anisimov A N, Farle M, Poulopoulos P, Platow W, Baberschke K, Isberg P, Wäppling R, Niklasson A M N and Eriksson O 1999 *Phys. Rev. Lett.* **82** 2390
[24] Isberg P, Hjörvarsson B, Wäppling R, Svedberg E B and Hultman L 1997 *Vacuum* **48** 483
[25] Anisimov A N, Platow W, Poulopoulos P, Wisny W, Farle M, Baberschke K, Isberg P, Hjörvarsson B and Wäppling R 1997 *J. Phys.: Condens. Matter* **9** 10581
[26] Lindner J *et al* 2002 to be published
[27] Scherz A, Wende H, Poulopoulos P, Lindner J and Baberschke K 2001 *Phys. Rev.* B **64** 180407(R)
see also the contribution of
Wende H, Sherz A, Wilhelm F and Baberschke K 2003 *J. Phys.: Condens. Matter* **15** S551
[28] Bürgler D E, Buchmeier M, Cramm S, Eisebitt S, Gareev R R, Grünberg P, Jia C L, Pohlmann L L, Schreiber R, Siegel M, Qin Y L and Zimina A 2003 *J. Phys.: Condens. Matter* **15** S443
[29] Pelzl J, Meckenstock R, Spoddig D, Schreiber F, Pflaum J and Frait Z 2003 *J. Phys.: Condens. Matter* **15** S451